Translocation of the pAntp Peptide and Its Amphipathic Analogue AP-2AL†

Guillaume Drin,‡,§ Hélene Déméné,§ Jamal Temsamani,‡ and Robert Brasseur*,||

Synt:em, Parc Scientifique Georges Besse, 30000 Nîmes, France, Centre de Biochimie Structurale, Faculté de Pharmacie, Montpellier I, France, and Centre de Biophysique Moléculaire Numérique, Faculté Universitaire des Sciences Agronomiques de Gembloux, 5030 Gembloux, Belgium

Received August 25, 2000; Revised Manuscript Received November 8, 2000

ABSTRACT: The pAntp peptide, corresponding to the third helix of the homeodomain of the Antennapedia protein, enters by a receptor-independent process into eukaryotic cells. The interaction between the pAntp peptide and the phospholipid matrix of the plasma membrane seems to be the first step involved in the translocation mechanism. However, the mechanism by which the peptide translocates through the cell membrane is still not well established. We have investigated the translocation ability of pAntp through a protein-free phospholipid membrane in comparison with a more amphipathic analogue. We show by fluorescence spectroscopy, circular dichroism, NMR spectroscopy, and molecular modeling that pAntp is not sufficiently helically amphipathic to cross a phospholipid membrane of a model system. Due to its primary sequence related to its DNA binding ability in the Antennapedia homeodomain−DNA complex, the pAntp peptide does not belong to the amphipathic α-helical peptide family whose members are able to translocate by pore formation.

Homeoproteins belong to a class of transactivating factors that bind to DNA through a specific sequence of 60 amino acids, the homeodomain. This latter sequence is structured in three α-helices with one *β*-turn between helixes 2 and 3 (*1*). Internalization experiments indicated that the homeodomain of Antennapedia is able to translocate across the plasmic membrane of nerve cells by a non-energy-dependent mechanism and to reach the nucleus (*2*). Mutations within the third helix of the homedomain suppress its internalization (*3*), and it has been established that a 16-amino acid long peptide, pAntp,[1] corresponding to this helix, is the minimal segment of the homeodomain capable of translocating through cell membranes (*4*). Further investigations have shown that the pAntp peptide enters into cells at 4 °C, demonstrating that peptide import does not involve endocytosis (*4*, *5*). Indeed, the internalization of pAntp is a receptor-independent process as indicated by the efficient cellular uptake of retro-, enantio-, and retro-inverso forms of this peptide (*6*, *7*). Others studies have shown that pAntp is internalized in vitro by several other cell lines comprising lymphocyte cells or aortic endothelial cells (*8*, *9*), suggesting that internalization is cell type-independent. Finally, it was indicated that pAntp, which is amphipathic, interacts with phospholipid membranes and adopts a partial α-helical structure in a membrane mimetic environment (*10*). In addition, the induction of a slight lamellar-to-inverted hexagonal phase transition by pAntp upon binding of a dispersion of brain phospholipid was observed (*10*).

These results suggest that the interaction between pAntp and cell membrane phospholipids is involved during the cellular import of this peptide. It was proposed that pAntp interacts with and translocates through the lipid bilayer by transiently forming inverted micelles (*11*, *12*). In this model, the peptide remains at the interface between the phospholipid bilayer and the aqueous environment. This may explain why polar compounds such as peptides (*13*−*16*) or oligonucleotides (*17*, *18*) covalently tagged to pAntp peptide enter into the cells. However, no experiments have been carried out to confirm whether the internalization mechanisms of these complexes and the peptide alone were similar.

Other basic amino acid-rich peptides such as transportan, a galanine−mastoparan chimeric peptide, TAT-derived peptides, and helical amphipathic model peptides are taken up by eukaryotic cells by a nonendocytic mechanism similar to those observed for pAntp (*5*, *19*, *20*). A recent structure−activity study indicated that the membrane-destabilizing propensities of designed helical amphipathic cell-permeable peptides cannot be correlated to their translocation activity (*5*). It was suggested that peptide−lipid interaction may only

† This work was supported by a grant from ANRT (Association Nationale pour la Recherche et la Technologie) to G.D., partially by the European Committee Research Program (Contract BIO-CT98-0227), by Anvar Languedoc Roussillon, and by the "Interuniversity Poles of Attraction Programme-Belgium State, Prime Minister's Office-Federal Office for Scientist, Technical and Cultural Affairs". R.B. is Directeur de Recherche at the FNRS.

* To whom correspondence should be addressed: Centre de Biophysique Moléculaire Numérique, Faculté des Sciences Agronomiques de Gembloux 2, rue Passage des Déportés, 5030 Gembloux, Belgium. Telephone: +32 (0)81 62 25 21. Fax: +32 (0)81 62 25 22. E-mail: brasseur.r@fsagx.ac.be.

‡ Synt:em.

§ Faculté de Pharmacie.

|| Faculté Agronomique.

[1] Abbreviations: CD, circular dichroism; DMF, dimethylformamide; DNS-PE, *N*-{[5-(dimethylamino)naphthyl]-1-sulfonyl}dipalmitoyl-L-α-phosphatidylethanolamine; LUVs, large unilamellar vesicles; MALDI-TOF MS, matrix-assisted laser desorption/ionization time-of-flight mass spectrometry; MD, molecular dynamics; MLVs, multilamellar vesicles; NBD-PE, *N*-{[7-nitrobenz-2-oxo-1,3-diazol-4-yl]dipalmitoyl}-L-α-phosphatidylethanolamine; NMR, nuclear magnetic resonance; POPC, 1-palmitoyl-2-oleyl-*sn*-glycero-3-phosphocholine; POPE, 1-palmitoyl-2-oleyl-*sn*-glycero-3-phosphoethanolamine; POPG, 1-palmitoyl-2-oleyl-*sn*-glycero-3-phosphoglycerol; *P*/*L*, peptide-to-lipid molar ratio; pAntp, RQIKIWFQNRRMKWKK-amide; AP-2AL, RQIKIWFQAARMLWKK-amide; RET, resonance energy transfer; SUVs, small unilamellar vesicles; TFE, 2,2,2-trifluoroethanol.

10.1021/bi002019k CCC: $20.00
Published on Web 01/18/2001

be the first step of a translocation mechanism which may involve other nonidentified proteic components (*5*, *9*). Understanding the internalization mode of pAntp could help shed light on the mechanism used to import these amphipathic peptides into cells.

We have, therefore, investigated the translocation ability of pAntp through a protein-free phospholipid membrane, i.e., the movement of this peptide from the outer to the inner leaflets. It was shown recently that several short α-helical amphipathic peptides, including mastoparan-X, a cell-permeable peptide, are able to translocate through phospholipid membranes by transiently forming peptide−lipid supramolecular pores (*21*−*23*). Another translocation mechanism has been described for the presequence of mitochondrial import of the cytochrome oxidase IV (p25) which crosses phospholipid membranes in a potential-dependent manner (*24*, *25*).

In this study, we have designed a peptide named AP-2AL by mutation of pAntp. This design was motivated by the necessity of having an analogue with physicochemical features similar to those of previously described translocating peptides. We have examined the lipid binding affinity, the membrane permeabilizing activity, and the translocation potency of pAntp and this analogue. Furthermore, we have investigated the secondary structure of both peptides by circular dichroism (CD) in membrane environments. The structure of the pAntp peptide and the AP-2AL peptide in SDS micelles was further examined by ^{1}H NMR spectroscopy. Finally, to explain the experimental results that were obtained, we have simulated the insertion and orientation of both peptides in a membrane using the IMPALA procedure, a Monte Carlo method associated with a restraint force field (*26*).

We report that pAntp cannot destabilize phospholipid membranes and cannot cross them at a low lipid-to-peptide molar ratio. The observed translocation of the analogue AP-2AL which is more ordered in α-helix than pAntp suggests that the latter is not sufficiently helically amphipathic to cross phospholipid membranes. Molecular modeling calculations confirm that pAntp remains at the surface of the membrane because it is not hydrophobic enough to penetrate deeply into the hydrophobic part of the membrane.

MATERIALS AND METHODS

Fmoc-PAL-PEG-PS (High Load) and 9-fluorenylmethyloxycarbonyl (Fmoc) amino acids were purchased from Perseptive Biosystems (Hamburg, Germany). Other reagents used for peptide synthesis included *N*,*N*′-diisopropylcarbodiimide (DIPCDI, Fluka), 1-hydroxybenzotriazole (HOBT, Perkin-Elmer), *N*,*N*-diisopropylethylamine (DIEA, Fluka), and dimethylformamide (DMF, Perseptive Biosystems).

The lipid POPC (1-palmitoyl-2-oleyl-*sn*-glycero-3-phosphocholine) and POPG (1-palmitoyl-2-oleyl-*sn*-glycero-3-phosphoglycerol) were obtained from Avanti Polar Lipids (Alabaster, AL). NBD-PE {*N*-[(7-nitrobenz-2-oxo-1,3-diazol-4-yl)diplamitoyl]-L-α-phosphatidylethanolamine}, DNS-PE (*N*-{[5-(dimethylamino)naphthyl]-1-sulfonyl}dipalmitoyl-L-α-phosphatidylethanolamine) and calcein were obtained from Molecular Probes (Eugene, OR). Sodium dithionite, 2,2,2-trifluoroethanol (TFE), and SDS were supplied by Sigma (St. Louis, MO). Sephadex G75 was purchased from Pharmacia Biotech (Uppsala, Sweden).

Peptide Synthesis. The peptides were synthesized according to the Fmoc-tBu strategy using an AMS 422 apparatus (ABIMED). Resin was washed with DMF and treated with a deprotecting mixture to cleave peptides from the resin and deprotect the side chains. Peptide purification was accomplished by reverse phase high-performance liquid chromatography (Water-prep LC 40, Waters) under 0.01% TFA/acetonitrile gradient conditions. The level of purification, as assessed by reverse phase analytical chromatography (Beckman Gold equipped with a diode array detector), was >95% for both peptides by the criterion of UV absorbance at 220 and 280 nm. The molecular masses were validated by MALDI-TOF spectrometry (Voyager Elite, Perseptive Biosystems).

Vesicle Preparation. For preparation of small unilamellar vesicles (SUVs), a lipid film with the desired composition was dried for 3 h and then suspended in buffer [20 mM Tris, 150 mM NaF, and 0.1 mM EDTA (pH 7.4)] to give a final concentration between 25 and 30 mM. The suspension was sonicated in ice-cold water for 25 min using a titanium tip ultrasonicator. Titanium and lipid debris were removed by centrifugation at 100000*g*. Dynamic light scattering measurements (Brookaven Instruments Ltd.) confirmed the existence of a single population of vesicles (mass content of >95%) with a mean diameter of 31 ± 1 nm. For preparation of large unilamellar vesicles (LUVs), the lipid suspension in buffer [20 mM Tris, 150 mM NaCl, and 1 mM EDTA (pH 7.4)] was frozen and thawed for five cycles and then extruded through polycarbonate filters (0.1 μm pore size) 21 times. The lipid concentration was determined in duplicate by phosphorus analysis as described in ref *27*.

Binding Isotherm. Fluorescence measurements were performed in 3 mL quartz cells at 25 ± 0.1 °C under constant magnetic stirring using a SLM AB-2 fluorometer (SLM Instruments, Inc., Urbana, IL). For measurement of the extent of peptide binding, excitation and emission wavelengths were set at 280 and 340 nm, respectively. Excitation and emission band-pass were set at 4 nm for both cases. Aliquots of a concentrated stock solution of LUVs (30 mM) were added to the peptide solution (1 μM). Each measurement was performed after the equilibrium had been reached. The contribution of scattered light to the observed signal was subtracted. The inner filter effect due to light scattering of the vesicles was corrected by the method of Lakowicz (*28*). The binding isotherms were analyzed as a partition equilibrium using the following formula:

$$X_b = K_p C_f$$

where X_b is defined as the molar ratio of bound peptide per total lipid, K_p corresponds to the partition coefficient, and C_f represents the equilibrium concentration of the free peptide in the solution. The curve resulting from plotting X_b versus the free peptide concentration, C_f, is referred to the conventional binding isotherm. To calculate X_b, the fraction of membrane-bound peptide f_b is determined with following the formula:

$$f_b = (F - F_0)/(F_\infty - F_0)$$

where F_0 is the fluorescence of the unbound peptide, F the fluorescence of the bound peptide, and F_∞ the fluorescence

signal obtained when all the peptide is bound to lipid. This latter value is extrapolated from a double-reciprocal plot of F (total peptide fluorescence) versus C_L (total concentration of phospholipid). With f_b known, the C_f value as well as the extent of peptide binding (X_b) could be calculated. Surface partition coefficients were calculated from the initial slope of each conventional binding isotherms (for details of the calculation, see ref *29*).

Dye Release. Dye-entrapped LUVs were prepared with a lipid film with the desired composition by using 70 mM calcein in buffer (the pH was adjusted to 7.4 with 1 M NaOH) as a hydrating solution. Calcein-entrapped vesicles were separated from free calcein on a Sephadex G75 column (18 cm × 1 cm). The release of calcein from LUVs was monitored by fluorescence at an emission wavelength of 520 nm (excitation wavelength of 490 nm). The maximum fluorescence intensity corresponding to 100% leakage was determined by the addition of 10% (w/v) Triton X-100 (10 μL) to 3 mL of the sample. The apparent percent leakage value was calculated according to the equation $100(F - F_0)/(F_{max} - F_0)$. F and F_{max} correspond to the fluorescence intensity before and after the addition of detergent, respectively. F_0 represents the fluorescence of the intact vesicles. The temperature was monitored at 25 ± 0.1 °C.

Measurement of Translocation. Symmetrically labeled LUVs were prepared by hydrating the lipid film composed of POPC, POPG, and DNS-PE (70:15:15 molar ratio). The observation of the fluorescence intensity of the Trp residue (336−340 nm) upon excitation at 280 nm allows us to monitor the resonance energy transfer (RET) from the Trp residue of the peptide to the dansyl fluorophore in the membrane. The temperature was controlled at 25 ± 0.1 °C.

Dithionite Ion Permeability. A lipid film composed of POPC, POPG, and NBD-PE (7:3:0.05 molar ratio) was resuspended with the buffer and frozen and thawed for five cycles. Small aliquots of the multilamellar vesicles (MLVs) were added to the buffer (control) or injected into a peptide solution in the presence of 10 mM sodium dithionite [freshly prepared at 1 M in 1 M Tris (pH 8.8)]. The fluorescence intensity of NBD at 530 nm (excited at 450 nm) was monitored at 25 ± 0.1 °C.

Circular Dichroism Measurement. Peptide CD spectra were obtained on a Jobin Yvon CD6 spectropolarimeter. The spectra were scanned at room temperature in a quartz optical cell with a 0.02 cm path length. Baseline spectra for each solvent or vesicle suspension were obtained prior to the peptide spectra. Each peptide was at a concentration of 1.5×10^{-5} M in buffer (150 mM NaF, 20 mM Tris, and 0.1 mM EDTA), in a TFE/buffer mixture (1:1, v/v) or in the presence of SDS (0.5%). To record spectra with SUVs, the peptide concentration was decreased to 5×10^{-6} M to ensure complete saturation with SUVs and to reduce the levels of absorption and diffusion caused by the presence of phospholipid vesicles. The helical content was determined from the mean residue ellipticity [Θ] at 222 nm according to the relation

$$[\Theta]_{222} = -30300[\alpha] - 2340$$

where [α] is the amount of helix (*30*).

^{1}H NMR Spectroscopy. The two-dimensional NMR experiments were performed on a Bruker AMX-400 spectrometer with a ^{1}H frequency of 400.130 MHz. Each peptide was dissolved in a $H_2O/^2H_2O$ (9:1, v/v) or $H_2O/^2H_2O$ (9:1 v/v)/[$^2H_{25}$]SDS mixture (100 mM) at pH 4.5. Measurements were performed at a peptide concentration of 3 mM. Formation of the peptide−micelle complex was monitored by the changes in chemical shifts of the peptide upon addition of the detergent to the peptide solution. All experiments were acquired with the transmitter set on the H_2O resonance. Solvent suppression was achieved by Watergate method (*31*) in association with water flip-back techniques (*32*). TOCSY (*33*, *34*), NOESY (*35*), and COSY experiments were recorded at 50 °C in the phase-sensitive mode. The TOCSY experiments used a mixing time of 50 ms, and the NOESY experiment used a mixing time of 60 or 100 ms. Data processing was performed on a HP workstation using GIFA (*36*). Prior to Fourier transformation, the FID was multiplied by a shifted sine-bell function in both dimensions and zero-filled to a final matrix of 512 × 1024 complex points.

Molecular Modeling. Peptides were built up using HyperChem (HyperCube, Inc.) assuming a perfect α-helix along the sequence. Molecules were energetically optimized using a conjugated gradient algorithm (rms = 0.1 kcal/mol) after a short MD simulation in vacuo (11 ps at 300 K, including 1 ps of a heating phase) using the all atom AMBER force field (*37*). The coordinate positions of atoms constituting the backbone were frozen to keep constant the ϕ and ψ angles associated with the helical conformation and to relax only the side chains during MD calculations. The penetration of the peptide into the phospholipid membrane was calculated by a Monte Carlo procedure using a simple restraint field (*26*). The lipid−water interfaces are described by a function, $C(z)$, which varies along the z-axis perpendicular to the plane of the membrane (the origin of the z-axis is the center of the bilayer).

$$C(z) = 0.5 - \frac{1}{1 + e^{\alpha(|z| - z_0)}}$$

$C(z)$ is an empirical function where α and z_0 are mathematical parameters calculated assuming $C_{(z=13.5Å)} = 0.49$ and $C_{(z=18Å)} = 0.49$ and that this symmetrical function is approximately constant from −∞ to −18 Å (hydrophilic phase), −13.5 Å to 13.5 Å (hydrocarbon core), and 18 Å to ∞ (hydrophilic phase). The molecule is translated so that this interface stays at $z = 13.5$ Å. A standard Monte Carlo procedure is applied at 308 K for 10^5 steps by randomly translating (maximum of 1 Å) and rotating (maximum of 5°) the peptide. The membrane−peptide interaction is estimated at each step by the restraint energy that is the sum of two terms (E_{int} and E_{lip}). The first one (E_{int}) increases when accessible hydrophilic atoms (i.e., $E_t > 0$) penetrate the membrane and decreases when accessible hydrophobic atoms do. This depends on the accessible surface in the peptide (S_i), the hydrophobicity [$E_{tr}(i)$], and the position (z_i) of each atom i:

$$E_{int} = -\sum_{i=1}^{N} S(i) E_{tr}(i) C(z_i)$$

E_{lip} accounts for the perturbation of the lipid bilayer due to

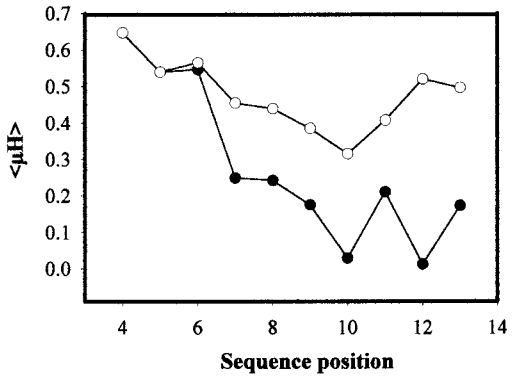

FIGURE 1: Plots of helical hydrophobic moment vs amino acid sequence for the pAntp peptide (●) and analogue AP-2AL (○). The hydrophobic moment was calculated for the seven-residue segment. The moment of each segment is plotted above the central fourth residue of that segment.

peptide insertion. It is defined as

$$E_{lip} = \alpha_{lip} \sum_{i=1}^{N} S(i)C(z_i)$$

where α_{lip} is an empirical factor fixed at -0.018. E_{lip} increases with the surface of the peptides in contact with lipids. Each calculation was carried out three times.

RESULTS

Design of the pAntp Analogue. The helical hydrophobic moment of the pAntp peptide (RQIKIWFQNRRMKWKK-amide) was calculated in seven-residue segments following the Eisenberg formula (*38*), with the hydrophobic scale of Fauchère and Pliska, based on the octanol−water partitioning of individual *N*-acetyl amino acid residues (*39*) and plotted versus sequence position (Figure 1). The region of the pAntp peptide with the maximal hydrophobic moment is the N-terminal half of the peptide. The hydrophobic moment decreases abruptly at position 7. On the basis of the observation that natural or designed membrane-active amphipathic peptides (*21*−*23*, *40*) have a helical hydrophobic moment approximately constant along their sequences, we have designed a mutant, named AP-2AL (RQIKIWFQAARM-LWKK-amide), with this characteristic. This peptide has a higher helical hydrophobic moment in the carboxy-terminal half than pAntp, resulting in a high helical hydrophobic moment along the sequence (Figure 1).

Interaction with the Membrane. The change in the Trp fluorescence intensity upon binding to phospholipid vesicles was used initially to demonstrate the interaction of the pAntp peptide with phospholipids (*10*) and to measure, in general, the lipid binding affinity of amphipathic peptides by determining their surface partition coefficients (*40*, *41*). Small aliquots of a concentrated stock solution of POPC/POPG (70:30 molar ratio) LUVs were added to the peptide (1 μM) in buffer, and the resulting increase in fluorescence intensity was plotted as a function of the lipid/peptide molar ratio (Figure 2A). The curves obtained by plotting X_b (the fraction of bound peptide per lipid) versus C_f (the equilibrium concentration of the free peptide in solution) are referred to the conventional binding isotherm (Figure 2B). The surface partition coefficients (K_p) of pAntp and AP-2AL were determined and were $\sim 13 \times 10^3$ and 106×10^3 M^{-1}, respectively. This indicates that the lipid-binding affinity of AP-2AL is higher than that of the pAntp peptide. We observed that the kinetics of lipid association of pAntp was instantaneous. However, the kinetics of lipid association of AP-2AL was biphasic with a rapid phase followed by a slow one when the lipid/peptide molar ratio was low (data not shown). The difference in the kinetics of binding between pAntp and AP-2AL peptides could not be due to a difference in oligomerization state prior to binding since both peptides are at a monomeric state at concentrations of <130 μM in buffer (data not shown). It is possible that the AP-2AL peptide interacts rapidly with the outer leaflet of LUVs and slowly crosses the membrane to interact with the inner leaflet. However, it should be noted that the value of K_p is proportional to the amount of accessible lipids (*29*). Thus, the higher lipid binding affinity of AP-2AL with respect to the lipid binding affinity of pAntp could reflect the fact that AP-2AL interacts with both leaflets of phospholipid vesicles and that pAntp interacts only with the outer leaflet.

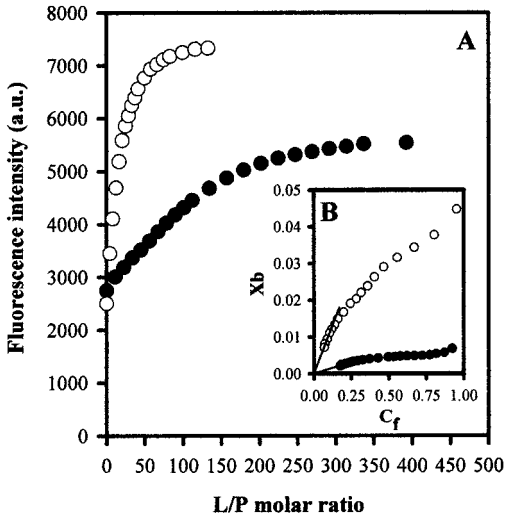

FIGURE 2: (A) Conventional binding curve of the pAntp peptide (●) and the AP-2AL peptide (○) on POPC/POPG (70:30) LUVs in buffer [20 mM Tris, 150 mM NaCl, and 1 mM EDTA (pH 7.4)] at 25 °C. (B) Binding isotherm of pAntp (●) and AP-2AL (○) on POPC/POPG (70:30) LUVs derived from the binding curve as described in Materials and Methods.

Permeabilization. The membrane permeabilizing activity of both peptides was examined by a dye release assay. An increase in fluorescence intensity due to the relief from the self-quenching of the dye molecule concentrated (70 mM) within the LUVs indicates dye release (Figure 3A). The relation between the apparent percent leakage and the peptide/lipid molar ratio was reported in Figure 3B and indicated that only AP-2AL induces a significant leakage of calcein from vesicles. Even at a very high peptide/lipid molar ratio (>1), pAntp cannot significantly permeabilize vesicles as indicated by a low percentage of leakage ($<10\%$).

Peptide Translocation. The translocation was detected by measuring the amount of untranslocated peptides remaining in the membrane outer leaflet of the membrane, according to the protocol described by Matsuzaki (*21*−*23*). The untranslocated peptides can be readily removed from the vesicle surface by extraction with a large excess of a second population of vesicles. The RET from the Trp residues of the peptide to the dansyl chromophore (DNS-PE) incorporated into the membrane of the first population of vesicles

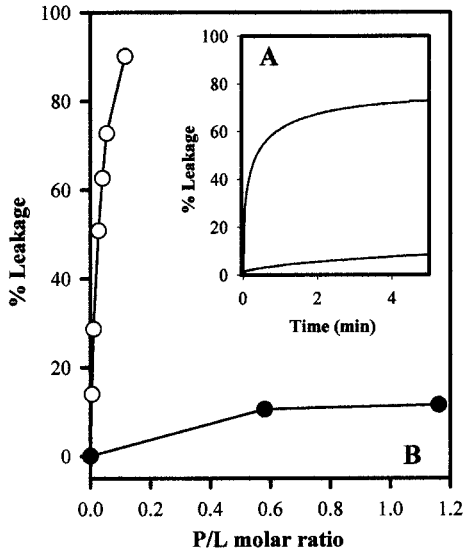

FIGURE 3: Membrane permeabilization induced by peptides. The level of membrane permeabilization was estimated by the percent leakage of calcein from POPC/POPG (70:30 molar ratio) LUVs. (A) Calceine release in the presence of pAntp (bottom trace; $P/L = 0.58$) and AP-2AL (top trace; $P/L = 0.054$). (B) The apparent percent leakage value after incubation for 5 min with pAntp (●) and AP-2AL (○) was plotted against the peptide/lipid molar ratio. Each value represents the average of triplicate experiments.

allows us to determine the unremovable fraction. At time zero, when dansyl-labeled vesicles (70 μM) were added to a peptide solution (1 μM), it resulted in a decrease in Trp fluorescence, indicating RET due to peptide binding to the membrane (Figure 4A). After incubation for 1 min, a second population of dansyl-free vesicles (DNS-PE was substituted with POPG) was added in large excess (more than 5-fold). The peptide molecules, which had been bound to the outer leaflet, were redistributed between the two vesicle populations, resulting in a relief from RET and a rapid increase in fluorescence intensity. In the case of AP-2AL, the increased fluorescence intensity was, however, smaller than the intensity obtained when both vesicle populations were simultaneously added to the peptide solution at time zero (as indicated by ΔF). This suggests that a fraction of the peptides became unexposed to the outer leaflet and therefore could not be transferred to the second vesicles. The final fluorescence decreases with the incubation time, indicating a time-dependent peptide translocation. It should be noted that the slow increase in fluorescence observed after addition of the second vesicle population could be attributed to the cross-back of peptides through the membrane of the first vesicle population (*21*, *22*).

The translocation assay of pAntp showed that no change in fluorescence was observed as a function of time (Figure 4B), implying that pAntp remains on the outer leaflet of the first population of vesicles and does not translocate through the phospholipid bilayer. This assay was carried out at a lipid/peptide molar ratio that was higher for pAntp than for AP-2AL to ensure that the fraction of lipid-bound peptide (calculated from binding experiment to be equal to 0.83) is similar to those calculated for the AP-2AL peptide (equal to 0.89). We also obtained a similar result at a lower peptide/peptide molar ratio (data not show).

To ensure the existence of AP-2AL translocation, we used a second protocol to demonstrate it (*22*, *23*). Figure 5 shows

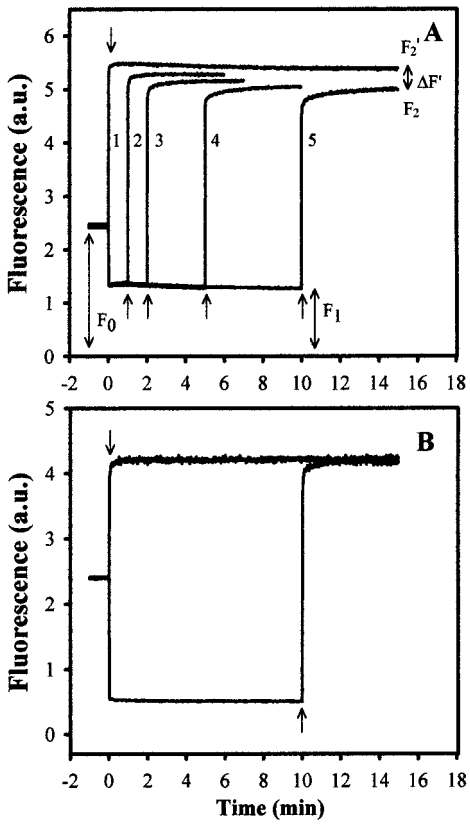

FIGURE 4: Detection of the peptide translocation. AP-2AL (A) or pAntp (B) was mixed with dansyl-LUVs (70:15:15 POPC/POPG/DNS-PE) at time zero. The peptide concentration was 1 μM, and the lipid concentrations were 70 and 350 μM for AP-2AL and pAntp, respectively. The fluorescence of Trp at 335 nm (excited at 280 nm) was measured. The peptide binding to the vesicle reduced the intensity from F_0 to F_1 due to RET. At various incubation times (1, 2, 5, and 10 min, traces 2−5, respectively), a large excess (final concentration of 470 μM for AP-2AL and 2.35 mM for pAntp) of a second population of dansyl-free LUVs (70:30 POPC/POPG) was added as indicated by the arrows. An increase in intensity indicates the relief from RET caused by the redistribution between the two vesicle populations of the peptide molecules which had been bound to the outer surface of the first vesicle. The difference (as labeled by ΔF) between the final fluorescence intensity (F_2) and the fluorescence intensity (F_2') when both populations of vesicles were simultaneously added at time zero indicates the fraction of peptide which is translocated into the inner leaflet during the incubation time. The trace is representative of five independent measurements.

that addition of sodium dithionite, a membrane-impermeable compound, to NBD-PE-containing MLVs quenches irreversibly the probe localized on the outermost leaflet. The addition of AP-2AL allowed the reducing ion to react with more than 85% of the NBD group within 6 min. If the peptide had permeabilized only the outermost bilayer, the reagent could have reacted with the fluorophore facing the first interlamellar space, having resulted in a level of quenching of <75% (*22*, *23*). This suggests that the AP-2AL molecule translocates across the outermost bilayer to destabilize the inner bilayer.

Secondary Structure of Peptides. The CD spectroscopy was used to determine the secondary structure of pAntp and AP-2AL in different media. In buffer, both peptides adopt a random conformation as indicated by a minimum at 198 nm (data not shown). In the presence of TFE (1:1 in buffer, v/v), the CD spectra of each peptide exhibited minima at 208 and 222 nm and a maximum at 193 nm, characteristic of a right-

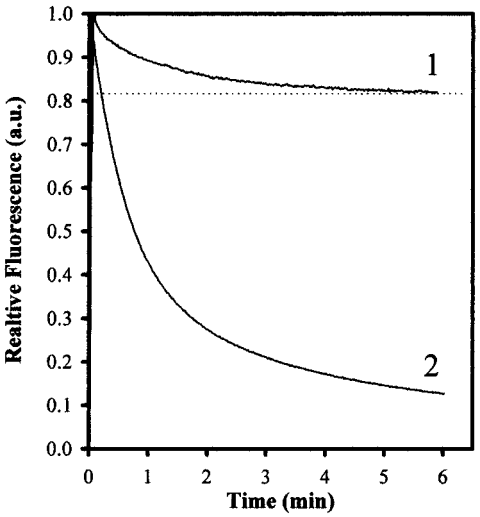

FIGURE 5: Detection of AP-2AL translocation. Small aliquots of MLVs composed of POPC, POPG, and NBD-PE (7:3:0.05) were added to buffer (trace 1) or to AP-2AL solution (trace 2) in the presence of 10 mM sodium dithionite. The membrane-impermeant $S_2O_4^{2-}$ quenches irreversibly NBD fluorescence by chemical reduction. The fluorescence at 530 nm (excitation at 450 nm) was normalized to the initial fluorescence in the absence of dithionite. The lipid concentration was 42 μM; the peptide concentration was 3 μM.

handed α-helical conformation (Figure 6A). However, the intensity of the band at 208 and 222 nm in the CD spectrum of pAntp was much reduced compared to the intensity of these bands in the CD spectrum of AP-2AL. We determined that the helical contents of pAntp and AP-2AL were equal to 34 and 43%, respectively. In the presence of SDS micelles (Figure 6B), the helical contents of pAntp and AP-2AL were equal to 40 and 49%, respectively. Finally, the secondary structure of the peptide upon binding to lipid vesicles was investigated by recording their CD spectra in the presence of POPC/POPG (70:30 molar ratio) SUVs (Figure 6C). In this environment, the helical content of both peptides was higher than those determined in other environments, indicating that the presence of phospholipids favors the α-helix conformation of these peptides. The helical contents of pAntp and AP-2AL were equal to 39 and 56%, respectively, indicating that the lipid-bound AP-2AL is more ordered in α-helix than the lipid-bound pAntp. However, the fractions of lipid-bound pAntp and AP-2AL at the lipid to peptide molar ratio used in the CD experiments, as estimated from the binding measurements, are equal to 0.82 and 1, respectively. Thus, the helical content of pAntp peptide corresponds, after correction, to 47%.

^{1}H NMR Analysis. Addition of SDS led to a drastic change in the ^{1}H chemical shift and line widths of both peptide proton resonances at 20 °C. The temperature of the peptide−micelle complex was increased to 50 °C to obtain peaks with acceptable line widths. We have carried out the sequential assignment of all the proton resonances following the standard method proposed by Wütrich (*42*) for two-dimensional NMR data analysis. TOCSY spectra were used to define the spin system, and NOESY spectra were used to identify inter-residue connectivities and to distinguish between equivalent spin systems. Assignments were obtained with the help of sequential NH(i)−NH(i+1), Hα(i)−NH(i+1) NOEs and NOE connectivities characteristic of the α-helical conformation. Figure 7 shows the Hα−NH region

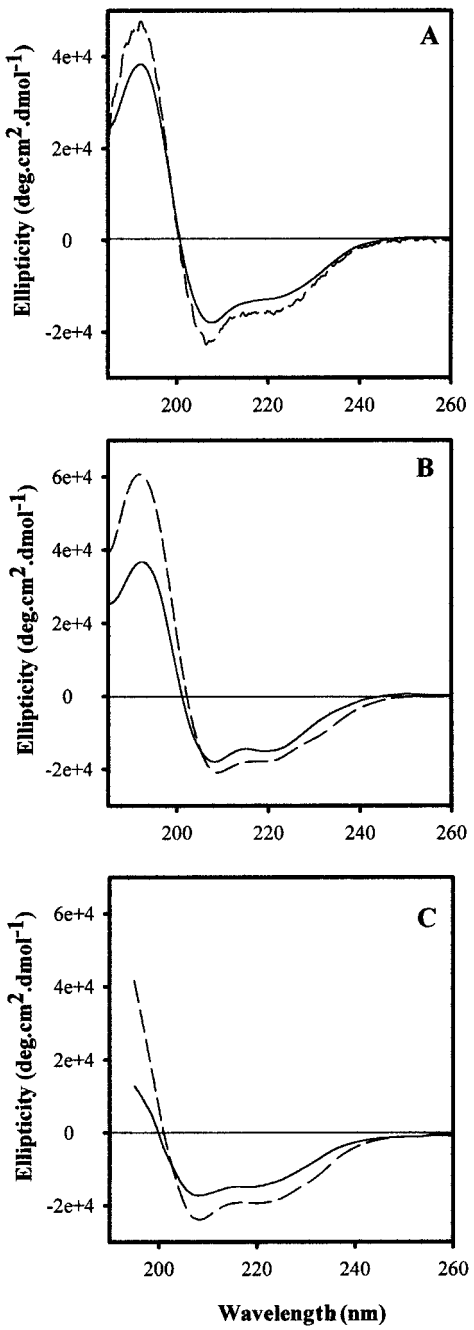

FIGURE 6: CD spectra (A) in 50% TFE (1:1, v/v) and (B) in the presence of SDS micelles. The peptide concentration was 150 μM in buffer [20 mM Tris, 150 mM NaF, and 0.1 mM EDTA (pH 7.4)], and the SDS/peptide molar ratio was 150. (C) CD spectra in the presence of POPC/POPG (70:30 molar ratio) SUVs with a lipid/peptide molar ratio of 325 (peptide concentration of 50 μM; lipid concentration of 16.3 mM): pAntp (—) and AP-2AL (− − −).

of the NOESY spectrum of each peptide in the presence of SDS micelles.

Due to the particular broad line width observed with both peptides in the presence of SDS, the $^3J_{NH-CH}$ coupling constant, useful for conformational analysis, could not be ascertained. Then, regular structure has been identified on the basis of the observation of sequential and medium-range NOEs and on the chemical shift variation of CαH protons. In the presence of SDS micelles, medium-range Hα(i)−Hβ-(i+3) and Hα(i)−NH(i+3) NOEs, corresponding to structuration of the peptide in α-helix, were observed for the amino-terminal half of the pAntp peptide from residues 3 to

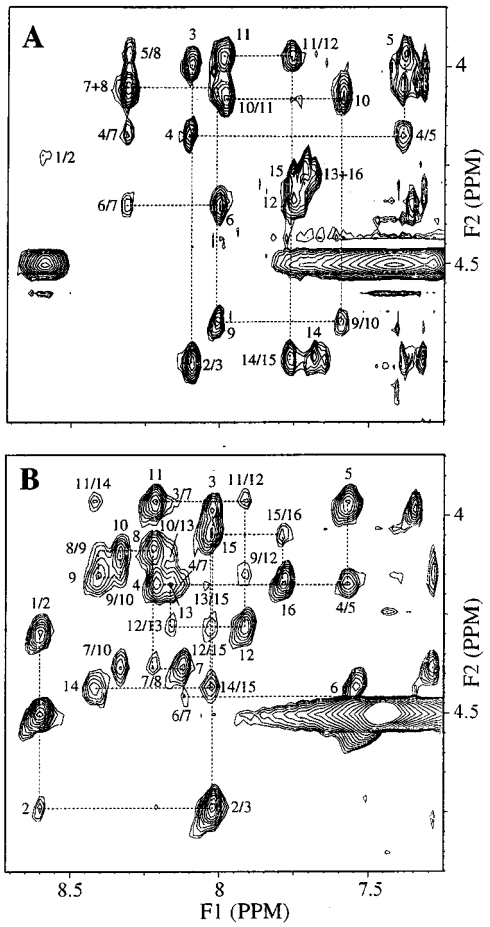

FIGURE 7: CαH−NH regions of the 60 ms mixing time NOESY spectrum of the pAntp peptide (A) and the AP-2AL peptide (B) in SDS micelles at pH 4.5 and 50 °C. Intraresidue NH−CαH cross-peaks are labeled with a single number. Medium-range and sequential NOE cross-peaks are labeled with two numbers indicating the residues contributing the CαH (F1 dimension) and NH (F2 dimension) protons, respectively. Sequential NOE cross-peaks are specifically indicated by the line joining cross-peaks due to consecutive residues (with the exception of the cross-peak between residues Arg1 and Gln2 and those which can be assessed unambiguously due to overlap).

9 (Figure 8A). In the same environment, we have identified for the AP-2AL peptide numerous Hα(*i*)−H*β*(*i*+3) NOEs in the segment of residues 3−12 and several Hα(*i*)−NH(*i*+3) NOEs for the segment of residues 4−15 (Figure 8B). However, several expected Hα(*i*)−NH(*i*+3) NOEs which could indicate the α-helical conformation of the peptide cannot be distinguished from sequential Hα(*i*)−NH(*i*+1) NOEs (Figure 7B). The CαH proton chemical shift values were used additionally to analyze the peptide structure. For both peptides, in the presence of SDS micelle, the deviations of the CαH chemical shift value from random coil values (*43*) are given in Figure 8 as a function of residue number. An α-helix structure is indicated by an upfield chemical shift of more than 0.1 ppm with respect to the random coil chemical shift value. The negative values were consistent with a helical conformation for residues 3−12 of the pAntp peptide. For the AP-2AL peptide, the negative values reflect the fact that this peptide adopts an α-helical structure from residue 3 to the C-terminus. These data suggest that the AP-2AL peptide is more ordered in an α-helix in a membrane-mimicking environment than pAntp and particularly in the carboxy-terminal half.

FIGURE 8: Summary of NMR data for the pAntp peptide (A) and the AP-2AL peptide (B) in SDS micelles at pH 4.5 and 50 °C. Sequential and medium-range NOE contacts observed in the 60 ms mixing time NOESY spectra of the peptide in SDS micelles are indicated by solid bars. NOEs corresponding to dashed bars are only observed for a mixing time of 100 ms. Asterisks denote NOEs whose presence or absence cannot be assessed due to overlap. The row labeled Δ*δ* shows the difference between the CαH chemical shift observed in SDS micelles and the random coil chemical shift values (*43*) as a function of residue position.

Simulation of Insertion of Peptides in the Membrane. We have simulated the insertion of both peptides in the membrane using the IMPALA procedure (*26*). To analyze the results of simulations, we have represented the energy as a function of the weight center of the molecule and the angle between the helix axis and surface plane (Figure 9). The pAntp peptide does not penetrate deeply into the membrane as indicated by a unique energy minimum corresponding to the localization of its weight center at 21.5 Å from the bilayer center associated with an angle of 12.6° (Figure 9A). The insertion of this peptide in the hydrophobic phase is energetically disfavored. In contrast, the AP-2AL peptide adopts several energetically favored configurations in the membrane as indicated by the four energetic local minima (states a, b, c, and d) shown in the energy contour map (Figure 9B). The best configuration corresponds to state c. Further analysis revealed that insertion of AP-2AL in the membrane from 22.25 (state a) to 6.25 Å (state d) is linked to the rotation of the peptide helix from 24.3 to −67.5°. Figure 10A shows a molecular representation of the different

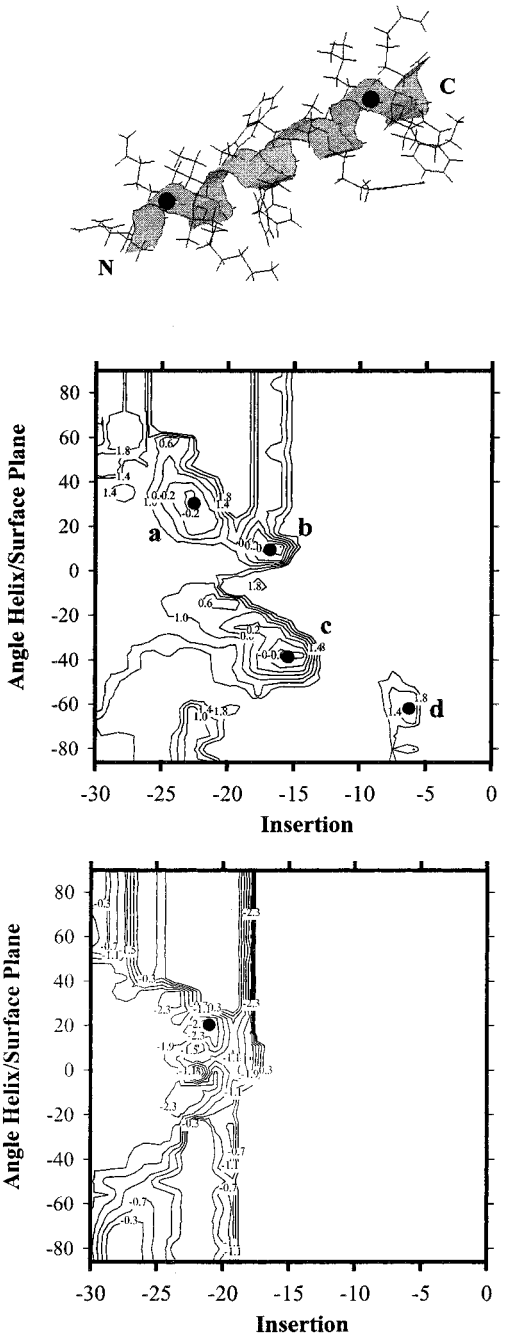

FIGURE 9: Energy contour maps of the peptide simulation by IMPALA. The energetic contour map corresponds to the miminal restraint energy (along the *z*-axis in kilocalories per mole) obtained during Monte Carlo vs peptide insertion (localization of the weight center) and peptide orientation defined by the angle between the helix axis and surface plane. The helix axis is subtended by two specified Nα atoms of the backbone (Nα atom of residue Ile3 and Nα atom of residue Trp14) represented by the solid black circle on the molecular representation of AP-2AL. (A) Energy contour map of pAntp. The solid dot represents the energetic minimum found for this peptide during calculations. (B) Energy contour map of AP-2AL. Each solid dot corresponds to a local energetic minimum [state a (insertion, −22.25 Å; angle, 24.3°), state b (insertion, −17 Å; angle, 9°), state c (insertion, −15.25 Å; angle, −37.8°), and state d (insertion, −6.25 Å; angle, −67.50°)].

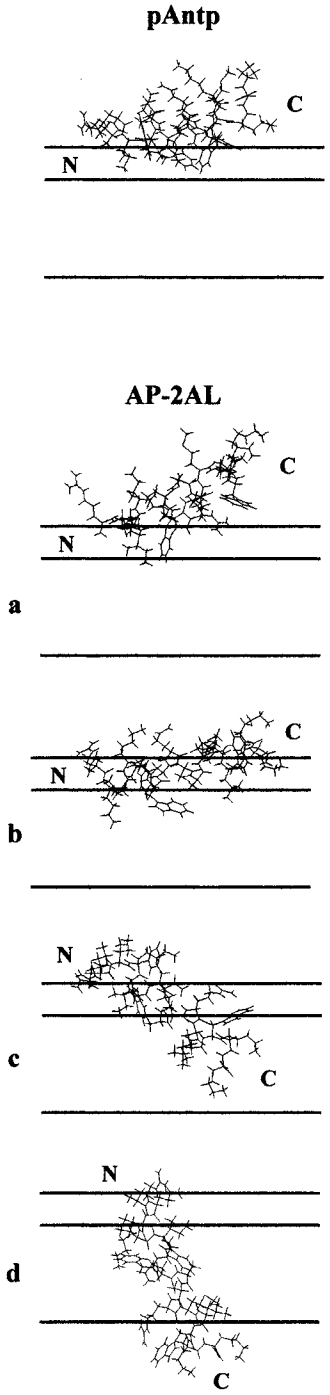

FIGURE 10: Molecular representation of peptide configurations in the membrane determined using IMPALA. (A) The best configuration of the pAntp peptide in the membrane. (B) Configurations of the AP-2AL peptide in the membrane, each one corresponding to a local minimum (a, b, c, or d).

configurations adopted by AP-2AL in the membrane and indicates that the carboxy-terminal half of AP-2AL penetrates first in the hydrophobic phase. The best configuration of pAntp corresponds to a localization of the peptide at the lipid−water interface, lying parallel to the membrane surface.

DISCUSSION

The cellular uptake of pAntp peptide is a rapid and efficient process that does not involve the endocytosis pathway and chiral receptor (*4*−*6*, *8*, *9*). On the basis of previous investigations, it was proposed that the pAntp peptide crosses rapidly the phospholipid matrix of the plasma membrane via a transient membrane destabilization step (*10*−*12*). We have, therefore, investigated the pAntp translocation potency using protein-free phospholipid vesicles, a suitable model membrane for assessing the translocation of amphipathic helical peptides (*21*−*25*).

We have designed an analogue named AP-2AL with a higher helical hydrophobic moment and a higher hydrophobicity than pAntp. The former is more similar in terms of amphipathicity to well-known membrane-active peptides (*44*) than the latter. We report first that both pAntp and AP-2AL interact with phospholipid vesicles. However, pAntp does not significantly modify the membrane permeability, even at low lipid/peptide ratios, indicating that pAntp cannot either form pores or destabilize membranes by acting as a detergent. In contrast, the AP-2AL analogue induces dye leakage of negatively charged vesicles at a similar lipid/peptide molar ratio found for peptides such as mastoparan-X (*22*). Indeed, the first translocation assay allowed us to show that AP-2AL rapidly crosses the phospholipid membrane as confirmed by the second translocation assay. In contrast, the pAntp peptide does not translocate through the phospholipid bilayer. The higher lipid binding affinity of the AP-2AL peptide with respect to pAntp may reflect the fact that the former interacts with both leaflets of the membrane and that the latter interacts only with the outer leaflet. Thus, these data suggest that the realized mutations allow pAntp to cross the phospholipid bilayer.

It could be envisaged that the AP-2AL peptide translocates through the membrane by pore formation. First, a significant permeabilization occurs at a relatively high lipid/peptide molar ratio. In addition, the 90° light scattering measured at 400 nm increases by only a few percent at the lipid/peptide molar ratio in which permeabilization and translocation occur (data not shown). These observations prove that membrane permeation does not involve micellization of the lipid bilayer and does not correspond to a "carpet" model. This latter model assumes the disintegration of the membrane after the formation of a peptide layer covering entirely the outer leaflet of the vesicle (*45*, *46*). However, it is possible that AP-2AL permeabilizes and crosses the membrane following a mechanism close to the carpet mechanism by forming a transient toroidal pore (*46*−*48*). Indeed, the relationship between membrane permeabilization kinetics and translocation (data not shown) implies that AP-2AL peptide translocation depends on the pore formation as described for several helical pore-forming peptides (*21*−*23*). Finally, light scattering experiments mentioned above indicate that translocation and permeabilizing activity of the AP-2AL peptide cannot be related to membrane fusion (*23*).

We have then investigated the influence of mutations on the structure of membrane-bound pAntp. First, structural investigations point out the fact that the pAntp (biotinylated at the N-terminus) adopts, in SDS micelles, a partial secondary structure, namely, a stable helix from the N-terminus up to amino acid 8 and an unordered structure from residue 9 to the C-terminus (*10*). Our structural data concerning pAntp (free at the N-terminus) in the same membrane-mimicking environment corroborate this observation.

The loss of structure in the middle of the peptide sequence seems to be related to the decrease in the amphipathic hydrophobic moment starting at this point. Determination of the helical content of AP-2AL by CD with respect to pAntp indicated that mutations increase the helical content of pAntp in a membrane mimetic environment or in the presence of negatively charged phospholipid vesicles. Our structural investigations by ^{1}H NMR spectroscopy revealed that AP-2AL should be ordered in a α-helix from residue 3 to the C-terminus in SDS micelles. Thus, structural differences determined by ^{1}H NMR between pAntp and AP-2AL peptides suggest that substitution of three polar residues with hydrophobic ones, which increases the helical hydrophobic moment of the carboxy-terminal half of the peptide, results in an increase in the helicity of this segment in a membrane-mimicking environment. SDS micelles are amphiphilic structures comparable to liposomes and are well-suited for the determination of the secondary structure of membrane-bound amphipathic peptides (*49*, *50*). For each peptide, the helical content determined upon binding of negatively charged vesicles and in the presence of SDS micelles differs slightly, indicating that the structure of both peptides determined by ^{1}H NMR spectroscopy is comparable to the structure of membrane-bound peptides. Thus, the permeabilization and translocation activity of AP-2AL could be correlated to its secondary structure.

To further understand the observed experimental differences between pAntp and AP-2AL peptides, we have simulated the penetration of both peptides into a phospholipid membrane using IMPALA. This procedure gives relevant insight on the energetically favored localization of amphipathic peptides in membranes (*26*). Simulations indicate that AP-2AL could penetrate deeper than pAntp into the membrane, the latter remaining at the water−lipid interface. The energetically favored configuration determined for both peptides is linked to the insertion of Trp residues in the membrane, corroborating well the fluorescence measurements. Analysis of the energy contour map of the AP-2AL peptide revealed the existence of a transition from a surface-lying state to a membrane-spanning state during the insertion of the peptide into the membrane. This transition was described for pore-forming peptides such as melittin and magainin 2 (*26*). Thus, the simulated transition agrees with the pore formation−translocation model that implies the transition between these two states (*48*). In addition, it could be envisaged that the energetic cost of the reorientation of the peptide in the membrane observed in our simulation could be compensated by an energetically favorable peptide−peptide interaction involved in the formation of multimeric pores. We conclude that these calculations are in agreement with the experimental observations and suggest that the low hydrophobicity of pAntp does not allow its insertion in the phospholipid bilayer. This is in agreement with a recent study that shows that the pAntp peptide interacts with the polar head of the negatively charged phospholipids but does not insert deeply into the lipid bilayer (*51*).

Taken together, these results indicate that the repartition between polar and hydrophobic amino acids along the third helix of the Antennapedia homedomain, related to its DNA binding ability, does not allow this segment to translocate through phospholipid membranes via a lipid-destabilizing mechanism. Two of the three substituted residues (Asn9 and Lys13) that block the translocation of the pAntp peptide are involved in molecular interactions with nucleotides in the Antennapedia homeodomain−DNA complex (*52*). Therefore, the expected translocation of pAntp does not occur when the peptide interacts with the phospholipid membrane because it is not sufficiently structurally amphipathic. Then, the helical amphipathicity, a structurally dependent parameter, does not seem to be related to the cell uptake of pAntp

peptide. This supports the demonstration that the helical structure is not required for cellular uptake of pAntp (*6*). Indeed, this means that pAntp does not enter into cells by the translocation mechanism proposed for the cell-permeable mastoparan-X (*22*).

Our data agree with previous work in which it was reported that pAntp interacts with phospholipid vesicles without changing the bilayer organization (*10*). Berlose and coworkers have indicated, however, that pAntp could induce a lamellar-to-hexagonal inverse lipid phase transition upon interacting with a lipid brain extract. This observation has been associated with the translocation ability of pAntp, and it was proposed that the cell membrane lipid composition is a triggering factor for pAntp translocation into cells (*10*). However, until now, the lipid composition appeared only as a modulator of membrane-destabilizing activity of positively charged amphipathic peptides (*53*, *54*). The permeabilizing potency of the AP-2AL peptide is effectively modulated by lipid composition as indicated by the calceine assay with a POPE/POPG instead of a POPC/POPG mixture. In contrast, the various vesicle phospholipid compositions that were tested do not allow us to observe a significant destabilizing activity associated with the pAntp peptide (data not shown).

It was demonstrated recently that although the nonendocytotic cellular uptake of designed amphipathic peptides requires helical amphipathicity as an essential property, the modulation of amphipathically associated parameters does not modify translocation activity of these peptides (*5*). The helical amphipathicity is a common feature of the membrane-destabilizing peptides (*43*, *45*, *55*). However, the modification of amphipathically associated parameters is known to influence the activity of these peptides (*43*, *55*). It was then suggested that entry of the peptide into cells does not imply membrane destabilization (*5*). Our results confirm that pAntp interacts with phospholipid membranes but suggest that pAntp cannot translocate by itself through a phospholipid membrane by pore formation. The partial amphipathicity of pAntp is probably only required for the interaction of this peptide with the phospholipid matrix of cell membranes. Thus, it may be envisaged that undefined factors are involved in the cellular uptake of the pAntp peptide as was proposed recently by another group (*5*, *9*).

ACKNOWLEDGMENT

We are indebted to Dr. F. Roux and Mrs. M. Paolini for peptide synthesis and purification, Dr. J. Sainte-Marie for help with phosphorus analysis, Dr. C. Braud for use of a circular dichroism spectropolarimeter, and Dr. M. Jullien for use of a photon correlation spectrometer. We are also thankful to Dr. Michel Kaczorek, Professor Anthony Rees, and Dr. Philippe Clair for helpful advice and criticism.

SUPPORTING INFORMATION AVAILABLE

Tables of ^{1}H chemical shifts of pAntp and AP-2AL. This material is available free of charge via the Internet at http://pubs.acs.org.

REFERENCES

1. Qian, Y. Q., Billeter, M., Otting, G., Müller, M., Gehring, W. J., and Wüthrich, K. (1989) *Cell 59*, 573−580.
2. Joliot, A., Pernelle, C., Deagostini-Bazin, H., and Prochiantz, A. (1991) *Proc. Natl. Acad. Sci. U.S.A. 88*, 1864−1868.
3. Le Roux, I., Joliot, A., Bloch-Gallego, E., Prochiantz, A., and Volovitch, M. (1993) *Proc. Natl. Acad. Sci. U.S.A. 90*, 9120−9124.
4. Derossi, D., Joliot, A., Chassaing, G., and Prochiantz, A. (1994) *J. Biol. Chem. 269*, 10444−10450.
5. Scheller, A., Oehlke, J., Wiesner, B., Dathe, M., Krause, E., Beyermann, M., Melzig, M. and Bienert, M. (1999) *J. Pept. Sci. 5*, 185−194.
6. Derossi, D., Calvet, S., Trembleau, A., Brunissen, A., Chassaing, G., and Prochiantz, A. (1996) *J. Biol. Chem. 271*, 18188−18193.
7. Brugidou, J., Legrand, C., Méry, J., and Rabié, A. (1995) *Biochem. Biophys. Res. Commun. 214*, 685−693.
8. Fenton, M., Bone, N., and Sinclair, A. J. (1998) *J. Immunol. Methods 212*, 41−48.
9. Oehlke, J., Scheller, A., Wiesner, B., Krause, E., Beyermann, M., Klauschenz, E., Melzig, M., and Bienert, M. (1998) *Biochim. Biophys. Acta 1414*, 127−139.
10. Berlose, J. P., Convert, O., Derossi, D., Brunissen, A., and Chassaing, G. (1996) *Eur. J. Biochem. 242*, 372−386.
11. Prochiantz, A. (1996) *Curr. Opin. Neurobiol. 6*, 629−634.
12. Derossi, D., Chassaing, G., and Prochiantz, A. (1998) *Trends Cell Biol. 8*, 84−87.
13. Hall, H., Williams, E. J., Moore, S. E., Walsh, F. S., Prochiantz, A., and Doherty, P. (1996) *Curr. Biol. 6*, 580−587.
14. Théodore, L., Derossi, D., Chassaing, G., Llirbat, B., Kubes, M., Jordan, P., Cneiweiss, H., Godement, P., and Prochiantz, A. (1995) *J. Neurosci. 15*, 7158−7167.
15. Mutoh, M., Lung, F. D., Long, Y. Q., Roller, P. P., Sikorski, R. S., and O'Connor, P. M. (1999) *Cancer Res. 59*, 3480−3488.
16. Bardelli, A., Longati, P., Williams, T. A., Benvenuti, S., and Comoglio, P. M. (1999) *J. Biol. Chem. 274*, 29274−29281.
17. Troy, C. M., Derossi, D., Prochiantz, A., Greene, L. A., and Shelanski, M. L. (1996) *J. Neurosci. 16*, 253−261.
18. Pooga, M., Soomets, U., Hällbrink, M., Valkna, A., Saar, K., Rezaei, K., Kahl, U., Hao, J., Xu, X., Wiesenfeld-Hallin, Z., Hokfelt, T., Bartfai, T., and Langel, U. (1998) *Nat. Biotechnol. 16*, 857−861.
19. Pooga, M., Hällbrink, M., Zorko, M., and Langel, U. (1998) *FASEB J. 12*, 67−77.
20. Vives, E., Brodin, P., and Lebleu, B. (1997) *J. Biol. Chem. 272*, 16010−16017.
21. Matsuzaki, K., Murase, O., Fujii, N., and Miyajima, K. (1995) *Biochemistry 34*, 6521−6526.
22. Matsuzaki, K., Yoneyama, S., Murase, O., and Miyajima, K. (1996) *Biochemistry 35*, 8450−8456.
23. Matsuzaki, K., Yoneyama, S., and Miyajima, K. (1997) *Biophys. J. 73*, 831−838.
24. Maduke, M., and Roise, D. (1993) *Science 260*, 364−367.
25. Leenhouts, J. M., Torok, Z., Mandieau, V., Goormaghtigh, E., and de Kruijff, B. (1996) *FEBS Lett. 388*, 34−38.
26. Ducarme, Ph., Rahman, M., and Brasseur, R. (1998) *Proteins 30*, 357−371.
27. Bartlett, G. R. (1959) *J. Biol. Chem. 234*, 466−468.
28. Lakowicz, J. R. (1983) in *Principles of Fluorescence Spectroscopy*, Plenum Press, New York.
29. Schwarz, G., Stankowski, S., and Rizzo, V. (1986) *Biochim. Biophys. Acta 861*, 141−151.
30. Chen, Y. H., Yang, J. T., and Martinez, H. M. (1972) *Biochemistry 11*, 4120−4131.
31. Piotto, M., Saudek, V., and Sklenar, V. (1992) *J. Biomol. NMR 2*, 661−665.
32. Lippens, G., Dhalluin, C., and Wieruszeski, J. M. (1995) *J. Biomol. NMR 5*, 327−331.
33. Bax, A., and Davis, D. G. (1985) *J. Magn. Reson. 65*, 355−360.
34. Rance, M. (1987) *J. Magn. Reson. 74*, 557−564.
35. Macura, S., Huang, Y., Sutter, D., and Ernst, R. R. (1981) *J. Magn. Reson. 43*, 259−281.
36. Malliavin, T. E., Pons, J. L., and Delsuc, M. A. (1998) *Bioinformatics 14*, 624−631.

37. Weiner, S. J., Kollman, P. A., Nguyen, D. T., and Case, D. A. (1986) *J. Comput. Chem. 7*, 230−252.
38. Eisenberg, D., Weiss, R. M., and Terwilliger, T. C. (1982) *Nature 299*, 371−374.
39. Fauchére, J. L., and Pliska, V. E. (1983) *Eur. J. Med. Chem. 18*, 369−375.
40. Wieprecht, T., Dathe, M., Epand, R. M., Beyermann, M., Krause, E., Maloy, W. L., MacDonald, D. L., and Bienert, M. (1997) *Biochemistry 36*, 12869−12880.
41. Mishra, V. K., and Palgunachari, M. N. (1996) *Biochemistry 35*, 11210−11220.
42. Wütrich, K. (1986) *NMR of proteins and nucleic acids*, John Wiley and Sons, New York.
43. Wishart, D. S., Bigam, C. G., Holm, A., Hodges, R. S., and Sykes, B. D. (1995) *J. Biomol. NMR 5*, 67−81.
44. Dathe, M., and Wieprecht, T. (1999) *Biochim. Biophys. Acta 1462*, 71−87.
45. Gazit, E., Boman, A., Boman, H. G., and Shai, Y. (1995) *Biochemistry 34*, 11479−11488.
46. Shai, Y. (1999) *Biochim. Biophys. Acta 1462*, 55−70.
47. Ludtke, S. J., He, K., Heller, W. T., Harroun, T. A., Yang, L., and Huang, H. W. (1996) *Biochemistry 35*, 13723−13728.
48. Matsuzaki, K. (1999) *Biochim. Biophys. Acta 1462*, 1−10.
49. Chupin, V., Leenhouts, J. M., de Kroon, A. I. P. M., and de Kruijff, B. (1996) *Biochemistry 35*, 3141−3146.
50. Gesell, J., Zasloff, M., and Opella, S. J. (1997) *J. Biomol. NMR 9*, 127−135.
51. Bellet-Amalric, E., Blaudez, D., Desbat, B., Graner, F., Gauthier, F., and Renaud, A. (2000) *Biochim. Biophys. Acta 1467*, 131−143.
52. Fraenkel, E., and Pabo, C. O. (1998) *Nat. Struct. Biol. 8*, 692−697.
53. Matsuzaki, K., Sugishita, K., Ishibe, N., Ueha, M., Nakata, S., Miyajima, K., and Epand, R. M. (1998) *Biochemistry 37*, 11856−11863.
54. Polozov, I. V., Polozova, A. I., Tytler, E. M., Anantharamaiah, G. M., Segrest, J. P., Woolley, G. A., and Epand, R. M. (1997) *Biochemistry 36*, 9237−9245.
55. Epand, R. M. (1998) *Biochim. Biophys. Acta 1376*, 353−368.

BI002019K